AFRL-AFOSR-VA-TR-2018-0321

Atomically Precise Metal Nanoclusters: Structure, Dynamics and Catalysis

Rongchao Jin
CARNEGIE MELLON UNIVERSITY

07/18/2018
Final Report

Air Force Research Laboratory
AF Office Of Scientific Research (AFOSR)/ RTB2
Arlington, Virginia 22203
Air Force Materiel Command

REPORT DOCUMENTATION PAGE

Form Approved
OMB No. 0704-0188

1. REPORT DATE *(DD-MM-YYYY)*	**2. REPORT TYPE**	**3. DATES COVERED** *(From - To)*
		15-Apr-2015 – 14 Apr 2018

4. TITLE AND SUBTITLE
Atomically Precise Metal Nanoclusters: Structure, Dynamics and Catalysis

5a. CONTRACT NUMBER

5b. GRANT NUMBER
FA9550-1 5- 1-0154

5c. PROGRAM ELEMENT NUMBER

6. AUTHOR(S)
Rongchao Jin

5d. PROJECT NUMBER

5e. TASK NUMBER

5f. WORK UNIT NUMBER

7. PERFORMING ORGANIZATION NAME(S) AND ADDRESS(ES)
Carnegie Mellon University
5000 Forbes Ave
Pittsburgh, PA 15213

8. PERFORMING ORGANIZATION REPORT NUMBER

9. SPONSORING / MONITORING AGENCY NAME(S) AND ADDRESS(ES)
USAF, AFRL DUNS 1 43574726
AF OFFICE OF SCIENTIFIC RESEARCH
875 NORTH RANDOLPH STREET, RM
ARLI NGTON VA 22203- 1954

10. SPONSOR/MONITOR'S ACRONYM(S)

11. SPONSOR/MONITOR'S REPORT NUMBER(S)

12. DISTRIBUTION / AVAILABILITY STATEMENT

DISTRIBUTION A: Distribution approved for public release.

13. SUPPLEMENTARY NOTES
none

14. ABSTRACT

We have fulfilled the central goal of our project, which is to investigate the structure and properties of atomically precise, ligand-protected metal nanoclusters in the size range from tens to hundreds of atoms. Such new materials have found major applications in catalysis for energy conversion, including CO_2 reduction to fuels and water splitting to H_2. The evolution of electronic and optical properties with cluster size is discovered to impact the catalytic reactivity. The correlations between the structure and catalytic reactivity have been mapped out. We have developed capabilities for controlling gold and bimetallic nanoclusters at the single-atom level (including heteroatom doping). Such capabilities are particularly important for designing atom-efficient new materials with tailored properties to meet specific energy and catalysis needs. Characterization of the atomic structures of nanoclusters enabled fundamental understanding of the mechanisms of the catalyzed reactions. Heteroatom substitution in gold nanoclusters allowed us to probe the atomic-level sensitivity of the nanocluster's electronic, optical and catalytic properties, and also to impart the nanocluster with new properties. We have gained insights into how the structure of nanocluster catalysts can be manipulated for catalytic processes. Such new insights will benefit rational design of highly efficient catalysts.

15. SUBJECT TERMS
Nanocluster, gold, bimetallic, structure, dynamics, catalysis

16. SECURITY CLASSIFICATION OF:			**17. LIMITATION OF ABSTRACT**	**18. NUMBER OF PAGES**	**19a. NAME OF RESPONSIBLE PERSON**
a. REPORT	**b. ABSTRACT**	**c. THIS PAGE**	UU		**19b. TELEPHONE NUMBER** *(include area code)*
U	U	U			

Standard Form 298 (Rev. 8-98)
Prescribed by ANSI Std. Z39.18

(Final Report)

Project Title: **Atomically Precise Metal Nanoclusters: Structure, Dynamics and Catalysis**
AFOSR grant #: FA9550-15-1-0154
Funding duration: April 2015 to April 2018
PI: Rongchao Jin
Contact Information: Department of Chemistry, 4400 Fifth Ave, Pittsburgh, PA 15213 (Phone: 412-268-9448 (o), Fax: 412-268-1061, Email: rongchao@andrew.cmu.edu)
Program Officer: Dr. Michael Berman

The central of our project is to investigate the structure and properties of atomically precise, ligand-protected metal nanoclusters in the size range from tens to hundreds of atoms. Such new materials hold promise in catalysis for energy conversion, and the evolution of electronic and optical properties with size fundamentally impact the catalytic reactivity of nanoclusters; thus, atomic-level control of nanoclusters is of paramount importance in both fundamental research and practical applications.

We have investigated gold nanoclusters ranging from Au_{10} to Au_{333} with atomic precision. We focused on the fundamental properties of such nanoclusters, including the atom-packing structures, electronic and optical properties, electrocatalytic reactivity and relationships with cluster size/structure. We have developed capabilities for controlling gold and bimetallic nanoclusters at the single-atom level (including heteroatom doping). Such capabilities are particularly important for designing atom-efficient new materials with tailored properties to meet specific energy and catalysis needs. Characterization of the atomic structures of nanoclusters enabled fundamental understanding of the mechanisms of the catalyzed reactions. Heteroatom substitution in gold nanoclusters allowed us to probe the atomic-level sensitivity of the nanocluster's electronic, optical and catalytic properties, and also to impart the nanocluster with new properties. The bimetallic nanocluster-based catalysts offer advantages resulting from the "synergy" of the base metal and a second metal. We have gained insights into how the structure of nanocluster catalysts can be manipulated for catalytic processes. Such new insights will benefit rational design of highly efficient catalysts.

Below we highlight some research achievements from the three-year project.

1. Nanocluster structure and ultrafast electron dynamics

The critical size—at which the metallic state is formed in metal nanoclusters—is of fundamental interest in nanoscience research. To map out the transition, we have investigated a series of sizes of gold nanoclusters. Our recent success is the attainment of the thiolate-protected $Au_{246}(SR)_{80}$ nanocluster (metal core diameter: 2.2 nm) (work reported in ***Science* 2016**). The particle structure can be divided into four parts. The inner most part is a Au_{116} decahedron exposing {111} facets at the two poles and {100} facets at the waist (Fig. 1A). The second part is a transition layer containing 90 gold atoms (Fig. 1B, magenta), which sphericizes the decahedron. These two parts together give rise to the Au_{206} core. The third part is the Au-S interfacial layer, in which the Au_{206} core is capped by the protecting motifs that fit the surface

features (such as facets and grooves) of the Au_{206} core. At the two poles of the core, the {111} facets are protected by –S–Au–S–Au–S– motifs and the {111}|{111} grooves are linked by simple bridging thiolates (Fig. 1B-C, bottom); at the waist the {100}|{100} and {111}|{100} grooves are all covered by –S–Au–S– staple motifs (Fig. 1B-C, top). The surface carbon tails (i.e. R groups) self-organize into two different types of patterns: pentagonal circles (termed as α-rotation) at the poles of the gold sphere and parallel pairs (termed as β-parallel) at the waist.

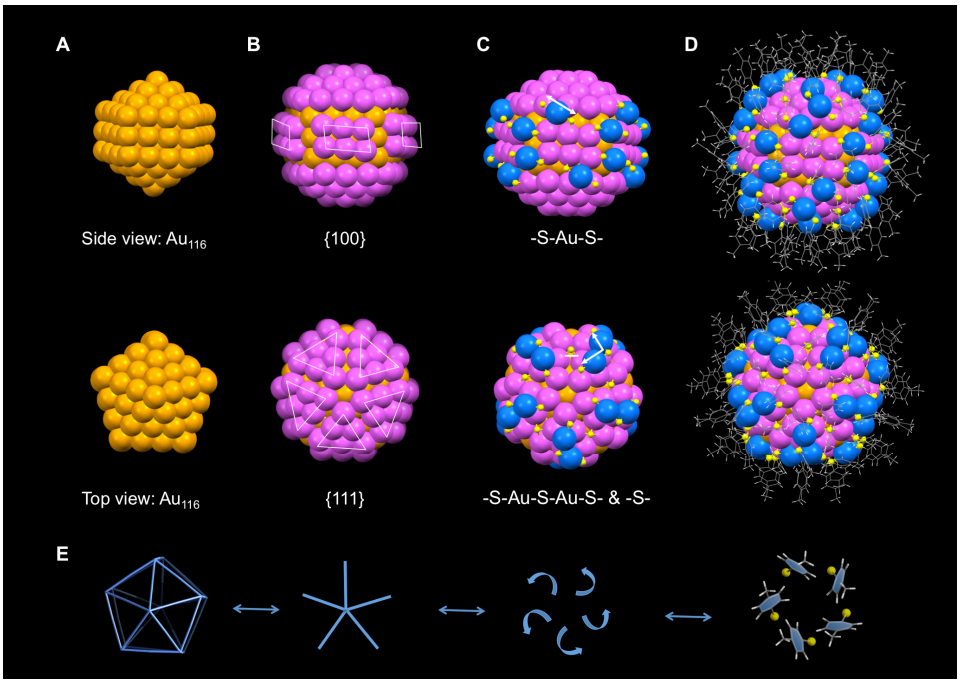

Figure 1. X-ray crystallographic structure of the 2.2 nm $Au_{246}(SR)_{80}$ nanocluster. (**A**) Au_{116} decahedral kernel (side and top views). (**B**) Transition layer comprising 90 gold atoms (magenta). (**C**) Gold-sulfur interfacial structure containing 20 monomeric staple motifs of –S–Au–S– (top), 10 dimeric staple motifs of –S–Au–S–Au–S–, and 10 bridging motifs of –S– (bottom). (**D**) Surface carbon layer and overall structure. (**E**) The emergence behavior in the nanocluster.

Electron dynamics measurements by femtosecond transient absorption spectroscopy indicate that the giant Au_{246} nanocluster is surprisingly non-metallic (***Angew Chem* 2017**). The steady-state optical absorption spectrum of $Au_{246}(SR)_{80}$ shows a peak at 470 nm and smaller peaks at various wavelengths (Fig. 2), indicating multiple excitonic absorption peaks, in contrast to the single plasmon band at ~520 nm for spherical nanoparticles. Transient absorption spectra of Au_{246} confirm the multiple excitonic peaks (Fig. 3B), rather than plasmonic bands, because the electron dynamics at these peak wavelengths are independent of the pump power (Fig. 3D), which are in contrast to the behavior of metallic gold nanoparticles.

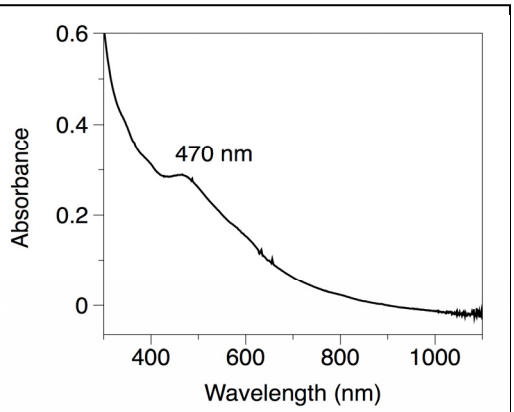

Figure 2. UV-vis absorption spectrum of the 2.2 nm $Au_{246}(SR)_{80}$ nanocluster.

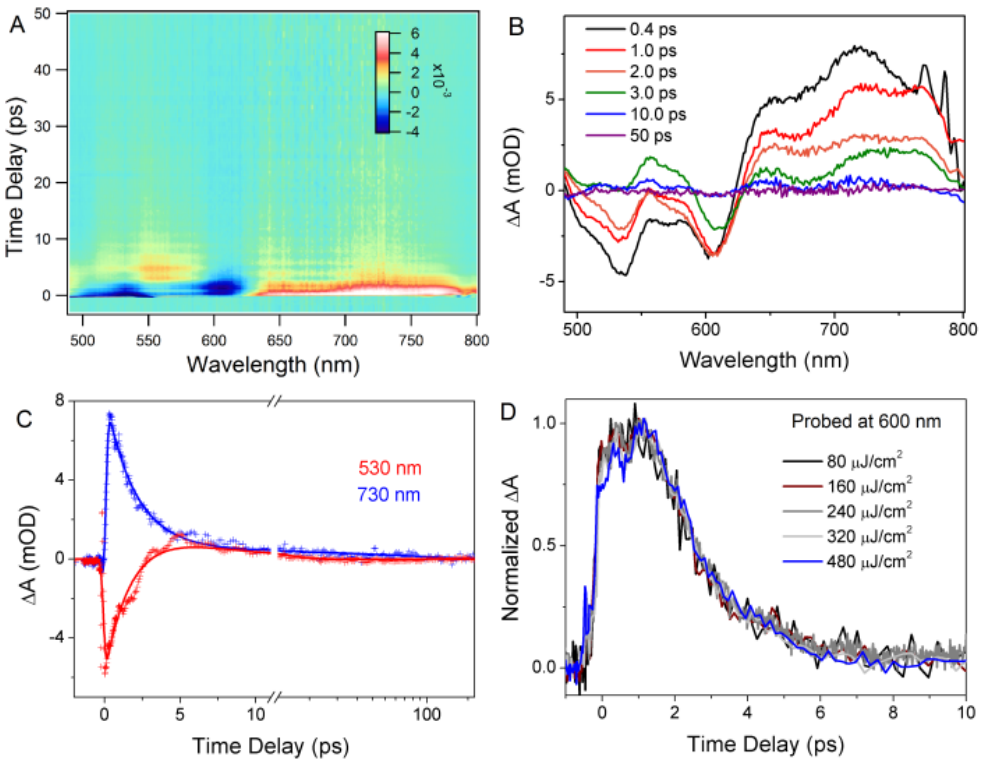

Figure 3. Ultrafast electron dynamics of Au_{246}. (A) Transient absorption data map between -3 ps and 50 ps with pump at 470 nm, with the red color representing excited state absorption (ESA) and the blue color representing ground state bleaching (GSB). (B) Transient absorption spectra as a function of time delay. (C) Kinetics and corresponding fits at selected wavelengths. (D) Normalized decay kinetics around 600 nm as a function of laser fluence with 470-nm pump.

In contrast to the non-plasmonic Au_{246} nanocluster, the 2.25 nm Au_{279} (***JACS* 2018**) and 2.5 nm Au_{333} (***Nat. Commun.* 2016**) both show a single plasmon band at ~530 nm (Fig. 4a, Au_{333} case), also confirmed by the transient absorption spectra (Fig. 4b), and the ultrafast electron dynamics starts to exhibit a power dependence (Fig. 4c) similar to conventional plasmonic NPs (Fig. 4d). These results unequivocally indicate the metallic bond starts to form in Au_{279}, Au_{333} and larger sizes. Taken together, our conclusion is that the metallic state is formed at 2.2 nm (between Au_{246} and Au_{279}); the mere 33-atom gap—over which a sharp transition occurs—is quite remarkable, which indeed goes against the theoretical prediction of a smooth transition over size (i.e., bandgap E_g~5.5 eV/n, where n is the number of gold atoms) by Kubo et al back in the 1960s.

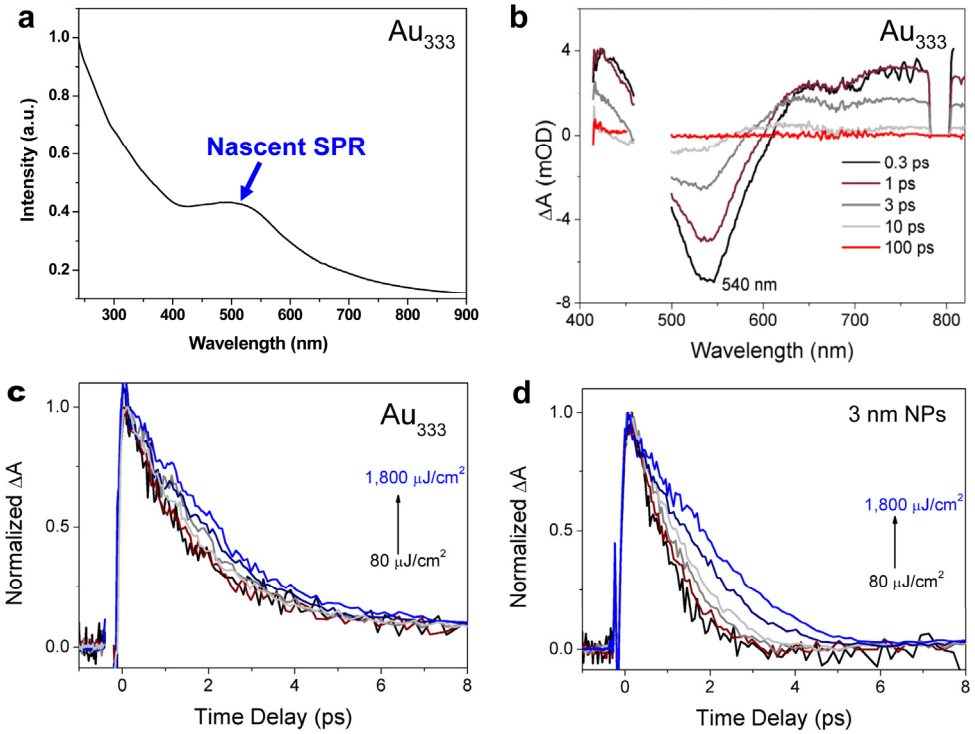

Figure 4. The emergence of metallic state in Au_{333}, a) stead-state optical absorption spectrum, b) transient absorption spectra, c) excitation power dependence, and d) comparison of Au_{333} with the 3 nm NPs.

2. Effect of non-metal to metal transition on catalysis

We futher investigated the impact of the transition on catalysis by choosing the 1) carbon monoxide (CO) oxidation and 2) electrocatalytic oxidation of alcohol, as the probe reactions (***Nat. Commun.* 2016**). We selected Au_{25}, Au_{38}, Au_{144} and Au_{333} as the catalysts (all protected by the same ligand, SCH_2CH_2Ph).

In the CO oxidation reaction, the CO conversion for each size of gold nanoparticles increases with temperature (Fig. 5a), and the size-dependent activity trend (Fig. 5b) indeed coincides with the transition from non-metallic to metallic state, with the most active size within the transition regime (i.e., between Au_{144} and Au_{333}, Au_{246} and Au_{279} not included due to different ligands). Previous work reported various trends of nanogold-catalyzed CO oxidation, but the precise size dependence was not clear due to the inherent polydispersity of those nanocatalysts. Different factors were invoked previously to explain the size dependence, with the highest activity attributed to the size that gives the longest interfacial perimeter distance between gold and oxide support, or the size that has more low-coordinated gold atoms. Our work indicates that the nonmetal to metal transition has a major influence on the catalytic reactivity of the nanoclusters. Interestingly, the effect is also found in the electrocatalytic oxidation of alcohol (Fig. 5c,d). Figure 5c shows the cyclic voltammetry (CV) profiles for Au_{25}, Au_{38}, Au_{144}, and Au_{333} (all supported on carbon black), respectively, in which the Au_{144} displays superior ethanol oxidation features with the highest current density in both forward oxidation and reverse oxidation peaks. Figure 5d compares the forward oxidation current density of the catalysts, where Au_{144} exhibits the best ethanol oxidation activity.

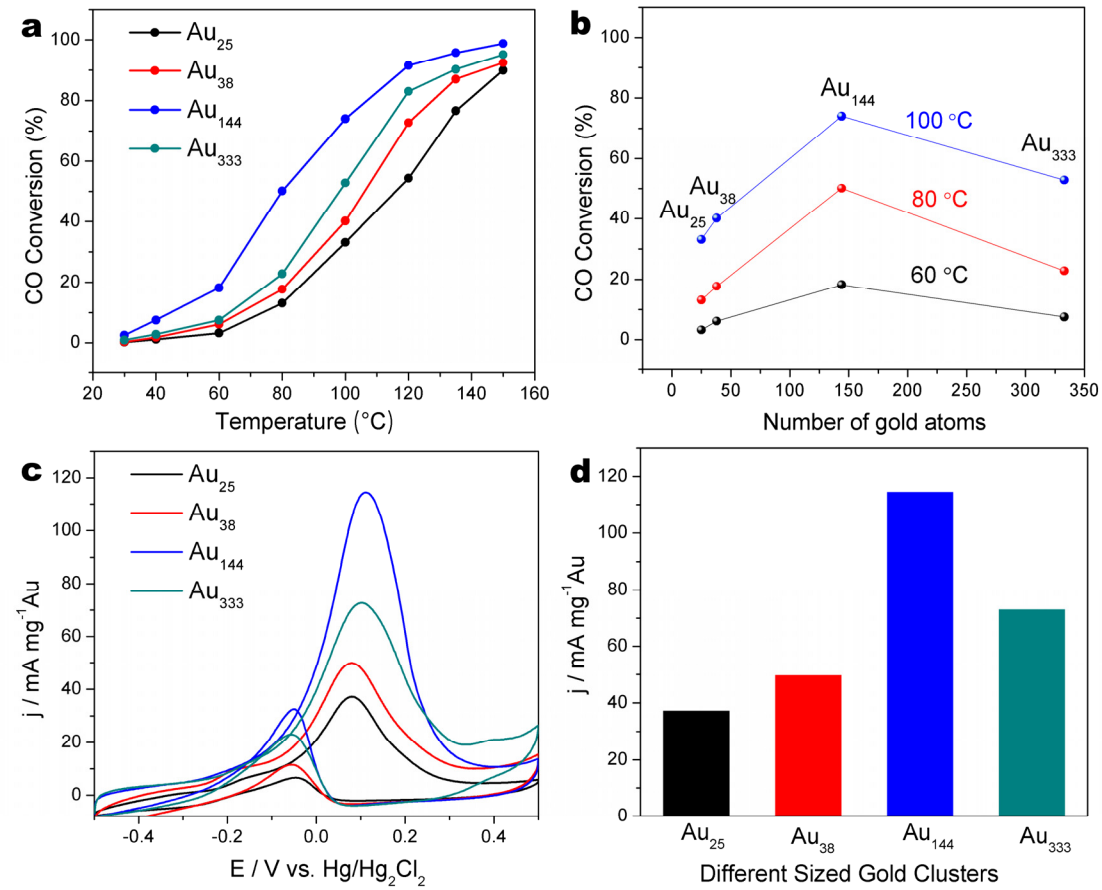

Figure 5. The impact of the transition on catalytic CO oxidation and electrochemical oxidation of alcohol. (a) The light-off curves of different sized nanoparticles, (b) a volcano-like trend of size effect, (c) Cyclic voltammetry (CV) profiles for different sized nanoparticles in deoxygenated 1 M KOH + 1 M CH_3CH_2OH solution, (d) Comparison of current density of different sized nanoparticles.

3. Electrocatalytic CO_2 conversion

The catalytic conversion of CO_2 into industrially relevant chemicals mitigates greenhouse gas emissions. In prior work, we discovered that Au_{25} nanoclusters exhibit excellent activity in electrocatalytic conversion of CO_2 to CO. We further integrated CO_2 conversion processes with carbon-free, renewable-energy sources to demonstrate the viability on larger scales (in collaboration with NETL). The Au_{25} nanoclusters were utilized as renewably powered CO_2 conversion electrocatalysts with CO_2 → CO reaction rates between 400 and 800 L of CO_2 per gram of catalytic metal per hour and product selectivities between 80 and 95%. These performance metrics correspond to conversion rates approaching 0.8–1.6 kg of CO_2 per gram of catalytic metal per hour. This proof-of-principle study provides some of the initial performance data necessary for assessing the scalability and technical

Carbon Negative CO_2 Conversion

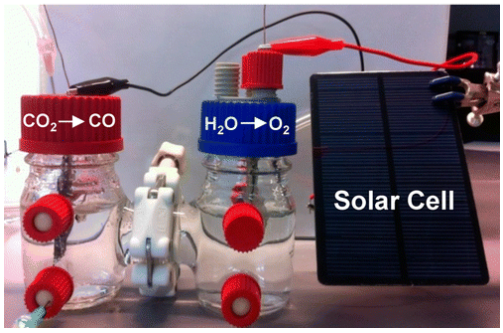

viability of electrochemical CO_2 conversion technologies. Specifically, we show the following: (1) all electrochemical CO_2 conversion systems will produce a net increase in CO_2 emissions if they do not integrate with renewable-energy sources, (2) catalyst loading vs activity trends can be used to tune process rates and product distributions, and (3) state-of-the-art renewable-energy technologies are sufficient to power larger-scale, tonne per day CO_2 conversion systems.

In recent work, we have investigated the atomic-level morphology effect of Au_{25} nanoclusters (sphere vs rod) as electrocatalysts for CO_2 reduction (work reported in ***ACS Catal*. 2018**). The distinctly different atomic-level morphology and charge states render the Au_{25} nanosphere higher activity in CO_2 reduction than the Au_{25} nanorod. At −0.67 V, the nanosphere cluster exhibits a higher FE (69.3% for CO) than that of the nanorod cluster (39.7%). DFT calculations based on their X-ray crystallographic structures revealed mechanistic insights for the observed difference in catalytic performance (Fig. 6). Specifically, the negative charge state of the nanosphere as well as the energetically favorable removal of -SCH_3 from the nanosphere to expose active sites contribute to the higher catalytic activity owing to the stabilization of the important *COOH intermediate. This work explicitly demonstrates that the atomic-level morphology and electronic properties can greatly influence the catalytic performance. The distinct morphology dependence of nanoclusters and the obtained mechanistic insights are expected to provide guidelines for future design of advanced catalysts for CO_2 reduction.

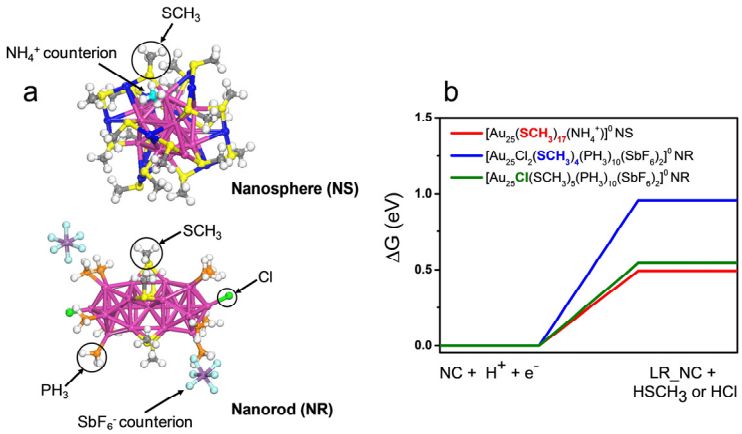

Figure 6. (a) Structures for the nanorod and the nanosphere in the presence of the NH_4^+ and SbF_6^- counterions, respectively. The circled regions on the nanoclusters demonstrate sites of ligand removal on the nanosphere (-SCH_3) and nanorod (-SCH_3, -Cl, and PH_3). (b) ΔG values for ligand removal (in eV) from the nanoclusters at 0 V vs RHE.

4. Electrocatalytic water splitting

Water splitting to produce hydrogen ($H_2O \rightarrow H_2$) is hampered by the other half reaction, $H_2O \rightarrow O_2$ (oxygen evolution reaction, OER). We have designed novel Au nanocluster/$CoSe_2$ composite catalysts for the OER half reaction (work reported in ***JACS* 2017**). Compared to plain $CoSe_2$ nanosheets, the $Au_{25}/CoSe_2$ composite exhibits largely enhanced OER performance by 2.5X. The $Au_{25}/CoSe_2$ composite also exhibits high stability in alkaline solution (with a mere ~11 mV increase of overpotential for 10 mA cm^{-2} after potential cycling for 1000 cycles), Fig. 7. To study the cluster size dependence for OER, we

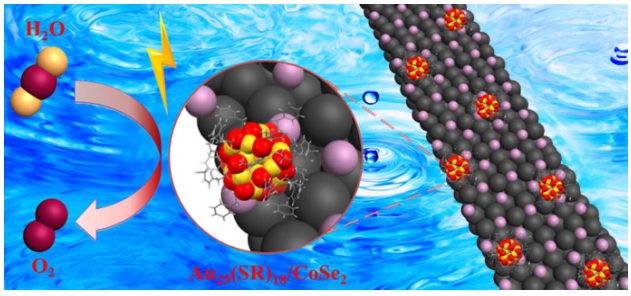

investigated Au_{25}, Au_{38}, Au_{144} and Au_{333} protected by the same ligand (i.e. phenylethanethiolate), as well as $Au_{10}(SPh\text{-}^{t}Bu)_{10}$. These nanoclusters were respectively loaded onto $CoSe_2$ (all at 2.0 wt%). The $Au_{10}/CoSe_2$, $Au_{144}/CoSe_2$ and $Au_{333}/CoSe_2$ catalysts were tested under the same conditions. The OER polarization curves (Fig. 7c) show a moderate increase of OER activity with an increase in cluster size. Fig 7d shows the size dependence of overpotential and current density, where the $Au_{333}/CoSe_2$ catalyst possesses the smallest overpotential (~0.41V for 10 mA cm^{-2}) and the largest current density of 15.44 mA cm^{-2} at the overpotential of 0.45 V. Based upon XPS measurements and DFT simulations, the activity enhancement is attributed to electronic interaction between Au nanocluster and the $CoSe_2$ support, which leads to the favorable formation of important intermediates OOH_{ad} at the $Au_n/CoSe_2$ interface.

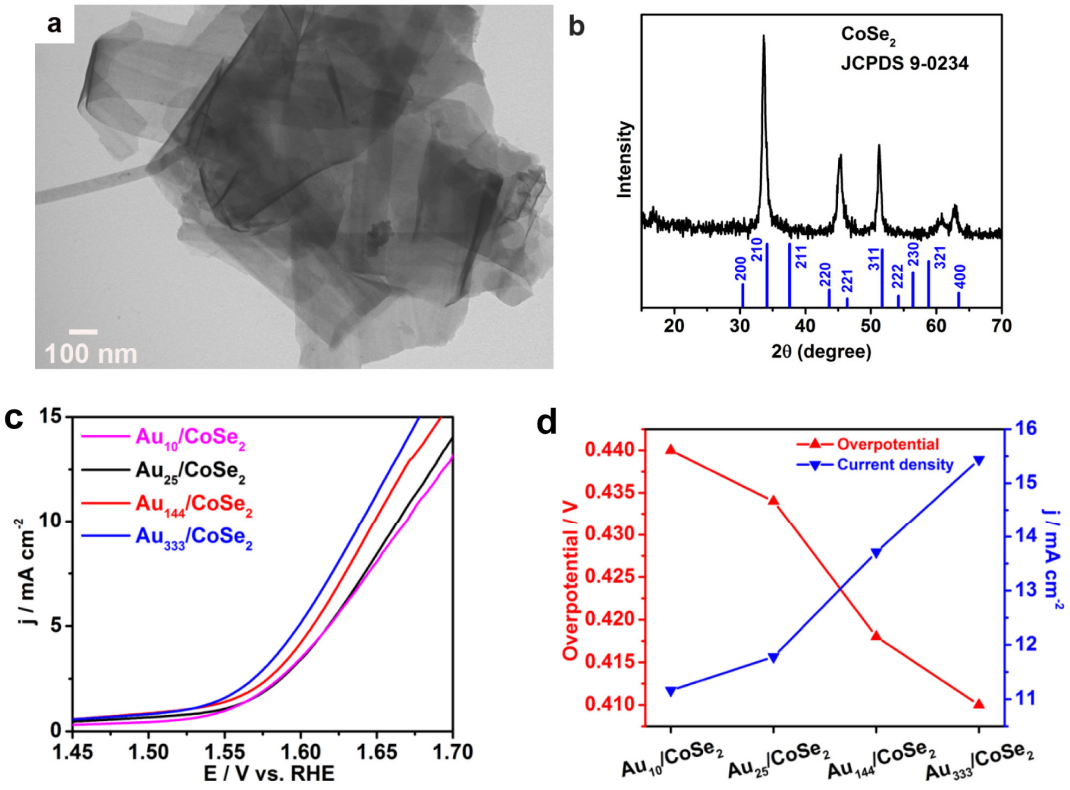

Figure 7. Water splitting at the cluster/$CoSe_2$ interface. (a) TEM image and (b) XRD pattern of $CoSe_2$ nanosheets, (c) OER polarization curves for $Au_n/CoSe_2$ catalysts, and (d) comparison of the overpotential required for achieving current density of 10 mA cm^{-2}, and the current density at overpotential of 0.45 V for $Au_n/CoSe_2$ catalysts.

We have also investigated the hydrogen evolution reaction (HER) over a composite catalyst, Au_{25}/MoS_2 (Fig. 8) (work reported in ***Small*** **2017**). Compared to plain MoS_2 nanosheets, the $Au_{25}(SR)_{18}/MoS_2$ nanocomposite exhibits enhanced HER activity with a smaller onset potential, at -0.20 V (vs RHE), and a higher current density of 59.3 mA cm^{-2} at the potential of -0.4 V (Fig. 8). Toward the mechanistic understanding, we have investigated Au_{25} clusters protected by thiolate vs selenolate (i.e. SPh vs SePh) as well as ligands of different length (including SC_6H_{13}, SC_8H_{17}, and $SC_{12}H_{25}$). An interesting result is the identification of the cluster/ligand interfacial

atom has a distinct effect on the HER activity, in addition to the interfacial interaction between nanoclusters and MoS_2. This work highlights the promise of metal nanoclusters in boosting the HER performance via tailoring not only the interfacial interactions between gold nanoclusters and MoS_2 nanosheets, but also the interface between metal core and surface ligands.

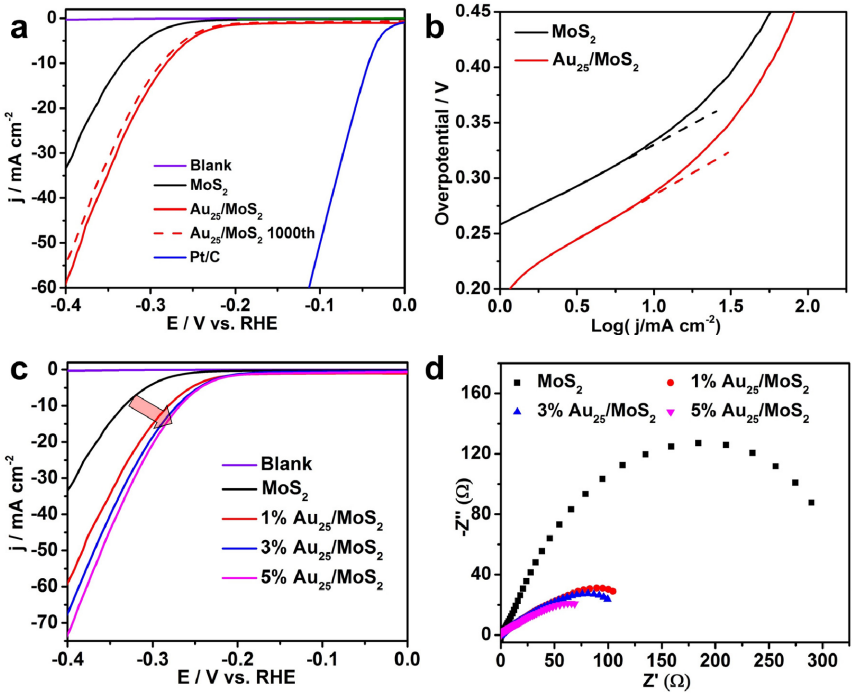

Figure 8. Electrocatalytic performance of the Au_{25}/MoS_2 catalyst. (a) HER polarization curves for Au_{25}/MoS_2, MoS_2, blank glassy carbon working electrode, Au_{25}/MoS_2 after the stability test and commercial Pt/C catalysts. (b) Tafel plots of Au_{25}/MoS_2 and MoS_2 catalysts. HER polarization curves (c) and impedance spectra (d) for MoS_2 and Au_{25}/MoS_2 with different loading amounts of Au_{25} nanoclusters.

5. Doping of gold nanoclusters and electron dynamics

Using the $Au_{25}(SR)_{18}$ nanocluster as a model system, we have investigated the doping chemistry (***Chem. Commun.*** **2016**). The silver atoms first go to the icosahedral shell (but not the icosahedral center), Figure 9a. Upon heavy doping of $Au_{25}(SR)_{18}$ nanocluster with silver through Ag(I)-SR complex, we found the Ag atoms indeed go to the surface staple-like motifs (Figure 9b).

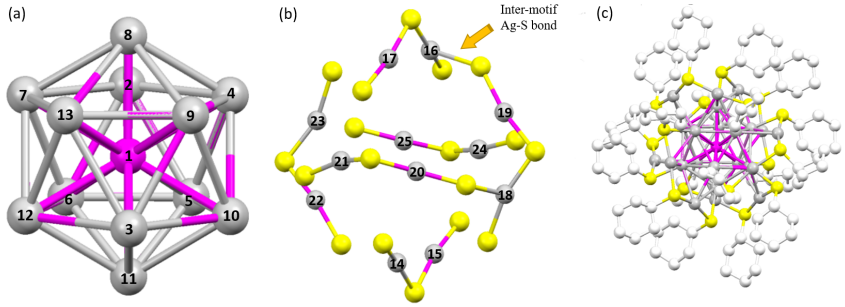

Figure 9. X-ray structure of the $Au_{25-x}Ag_x(SR)_{18}$. (a) The 13-atom icosahedral alloy core. (b) Six [−SR−Au(Ag)−SR−Ag−SR−] dimeric staples with different occupancy of Au/Ag atoms. (c) Total structure of $Au_{25-x}Ag_x(SR)_{18}^-$. Magenta: Au, gray: Ag/Au, yellow: S, grey: C.

In contrast, Pd and Pt dopants exclusively occupy the icosahedral center only, forming $M_1@Au_{24}(SR)_{18}$ (M=Pd, Pt) clusters. We have investigated the ultrafast relaxation dynamics of Pd/Pt doped clusters using femtosecond visible and near infrared transient absorption spectroscopy (work reported in ***Nanoscale* 2016**). Three relaxation components are identified for both mono-doped clusters (Fig 10): (1) sub-picosecond relaxation within the M_1Au_{12} core states; (2) core to shell relaxation in a few picoseconds; (3) relaxation back to the ground state in more than one nanosecond. Despite similar relaxation pathways for the two doped nanoclusters, the coupling between metal core and surface ligands is accelerated by over 30% in the case of Pt dopant compared with the Pd dopant. Compared to Pd doping, the case of Pt doping leads to much more drastic changes in the steady state and transient absorption (Figure 10) of the clusters. These results demonstrate that a single foreign atom can lead to entirely different excited state spectral features of the whole cluster compared to the parent $Au_{25}(SR)_{18}$ cluster.

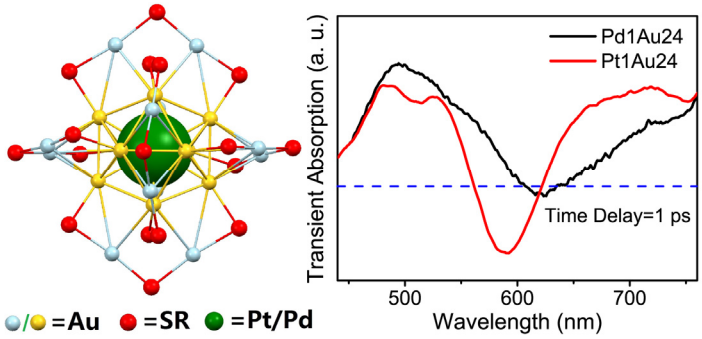

Figure 10. Transient absorption spectra of $M_1@Au_{24}(SR)_{18}$ (M=Pd, Pt) clusters.

6. Controlling nanocluster structures for understanding the structure-catalytic activity relationships

The structure of nanoclusters plays a critical role in dictating the material properties. Gold is well known to adopt face-centered cubic (FCC) structure. Significantly, we have succeeded in controlling the structure of Au_{38} to be body-centered cubic (BCC) (work reported in ***Angew. Chem.* 2015**). This nanocluster is composed of 38 gold atoms protected by 20 adamantanethiolate ligands and two sulfido atoms ($Au_{38}S_2(SR)_{20}$, where R = $C_{10}H_{15}$) as revealed by X-ray crystallography. This BCC structure is in striking contrast with the FCC structure of bulk gold and the bi-icosahedral structure of $Au_{38}(SCH_2CH_2Ph)_{24}$ (our previous work). The BCC nanocluster possesses a HOMO-LUMO gap of ~1.5 eV, much larger than that of the bi-icosahedral $Au_{38}(SCH_2CH_2Ph)_{24}$ (0.9 eV). The BCC gold nanocluster is further demonstrated to be more active in catalytic selective oxidation of sulfides (Table 1). In recent work, a hexagonal close-packed (HCP) nanocluster has also been attained, with the structure determined by X-ray crystallography (work reported in ***Angew. Chem.* 2016**). The HCP gold nanocluster consists of 30 gold atoms, with the cluster surface protected by 18 ligands of 1-adamantanethiolate.

Table 1. The catalytic performance of $Au_n(SR)_m$ nanoclusters supported on TiO_2 oxide in selective oxidation of methyl phenyl sulfide with PhIO.[a]

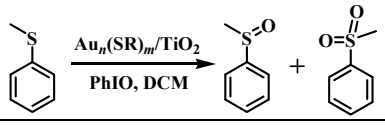

Entry	$Au_n(SR)_m$	Conv. [%][b]	Selectivity [%][b]	
			Sulfoxide	Sulfone
1	$Au_{25}(SC_6H_{13})_{18}$	72.6	98.8	1.2
2	biico-$Au_{38}(SC_6H_{13})_{24}$	77.2	99.1	0.9
3	bcc-$Au_{38}S_2$(S-Adm)$_{20}$	92.8	99.9	0.1

[a] Reaction conditions: 0.10 mmol methyl phenyl sulfide, 0.10 mmol PhIO, 0.5 mg $Au_n(SR)_m$ clusters supported on 50 mg TiO_2, 1 mL DCM, 35 ^oC, 8h; [b] The conversion of sulfide and selectivity of products were analyzed by ^1H NMR.

Beside the effect of crystalline phase on catalysis, in recent work we have also controlled the surface structure of 28-atom $Au_{28}(SR)_{20}$ nanoclusters using a ligand-based strategy (Figure 11) (work reported in ***JACS* 2016**). Two thermodynamically stable were obtained, i.e. Au_{28}(S-*c*-$C_6H_{11})_{20}$ (where –*c*-C_6H_{11}=cyclohexyl) and $Au_{28}(SPh\text{-}^tBu)_{20}$ (where -Ph-^{t}Bu = 4-*tert*-butylbenzyl), which possess the same FCC Au_{20} kernel but different surface structures (Figure 11). The intriguing ligand effect is further investigated via dispersion-corrected density functional theory calculations. The different surface structures are manifested in catalytic activity (e.g. CO oxidation, Figure 12A), but after the ligands are removed, the two clusters exhibit similar activity (Figure 12B) due to the bare Au_{28} clusters converging to the same structure.

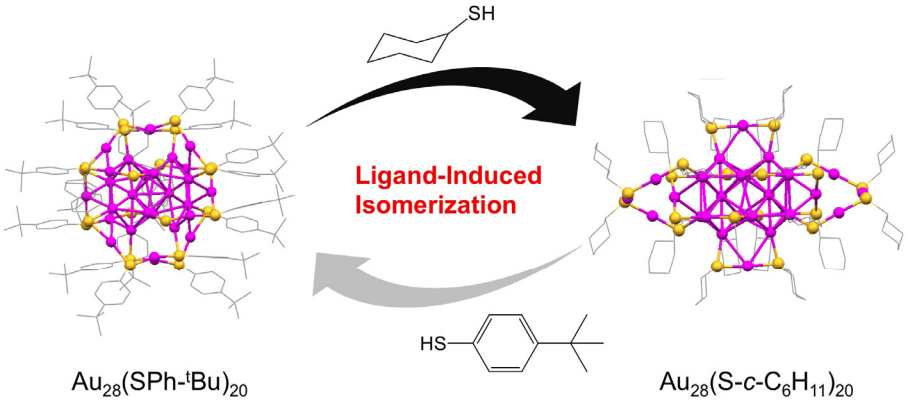

Figure 11. Structural control in **the case of** $Au_{28}(SR)_{20}$ with different R groups.

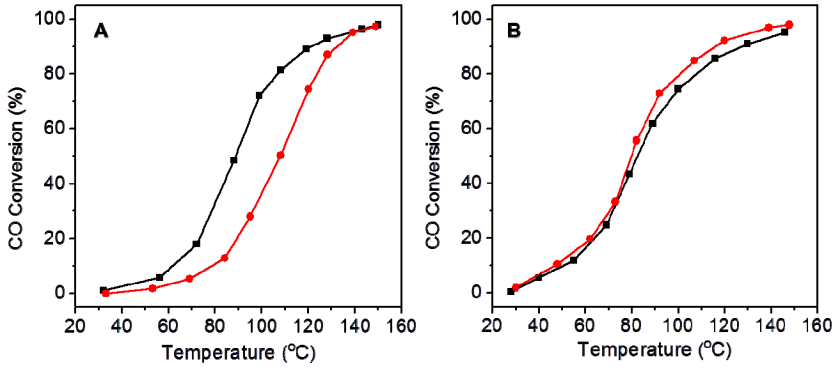

Figure 12. CO oxidation light-off curves of CeO_2 supported $Au_{28}(S\text{-}c\text{-}C_6H_{11})_{20}$ (black profile) and $Au_{28}(SPh\text{-}^tBu)_{20}$ (red) catalysts. (A) Catalysts pretreated with O_2 at 150 °C for 1 h; (B) pretreated with O_2 at 300 °C for 1 h to remove ligands.

7. Discovery of periodicity in nanoclusters

In very recent work, we have revealed for the first time the periodicities in nanoclusters (manifested in the formula, growth pattern and property evolution) (work published in ***JACS* 2016; *Science Advances* 2015**). A family consisting of $Au_{20}(TBBT)_{16}$, $Au_{28}(TBBT)_{20}$, $Au_{36}(TBBT)_{24}$, $Au_{44}(TBBT)_{28}$, and $Au_{52}(TBBT)_{32}$ nanoclusters gives rise to a neat "magic series" with a unified formula of $Au_{8n+4}(TBBT)_{4n+8}$ (n=2 to 6), Figure 13. Such a periodicity in magic numbers is a reflection of the uniform anisotropic growth patterns in this magic series (Figure 13), and the n value is correlated with the number of (001) layers in the face-centered cubic (fcc) lattice. The size-dependent quantum confinement nature of this magic series is further understood by an empirical scaling law and the classical "particle in a box" model, as well as the density functional theory calculations.

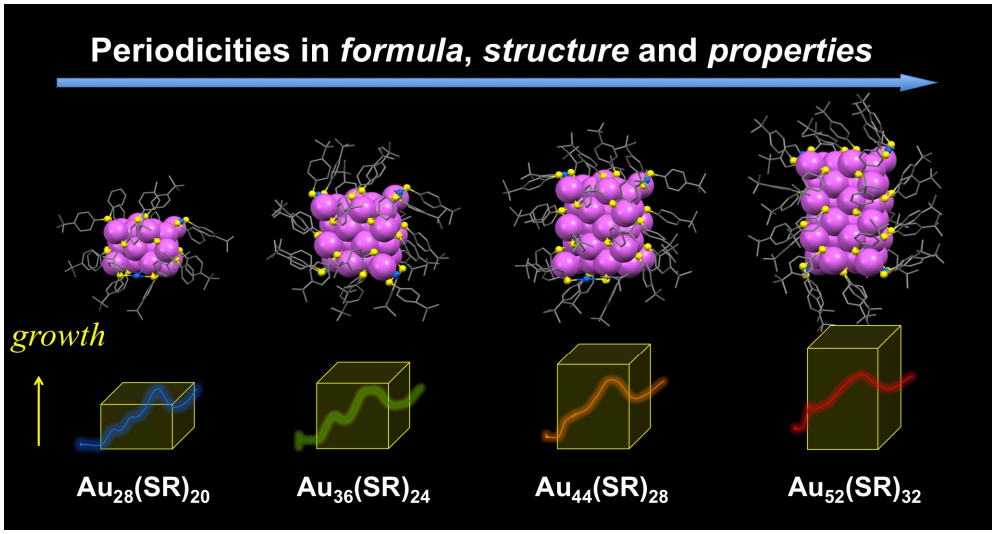

Figure 13. A magic-size series of gold nanoclusters protected by 4-*tert*-butyl-benzenethiolate (TBBT), including $Au_{28}(TBBT)_{20}$, $Au_{36}(TBBT)_{24}$, $Au_{44}(TBBT)_{28}$ and $Au_{52}(TBBT)_{32}$ with a uniform progression of $Au_8(TBBT)_4$.

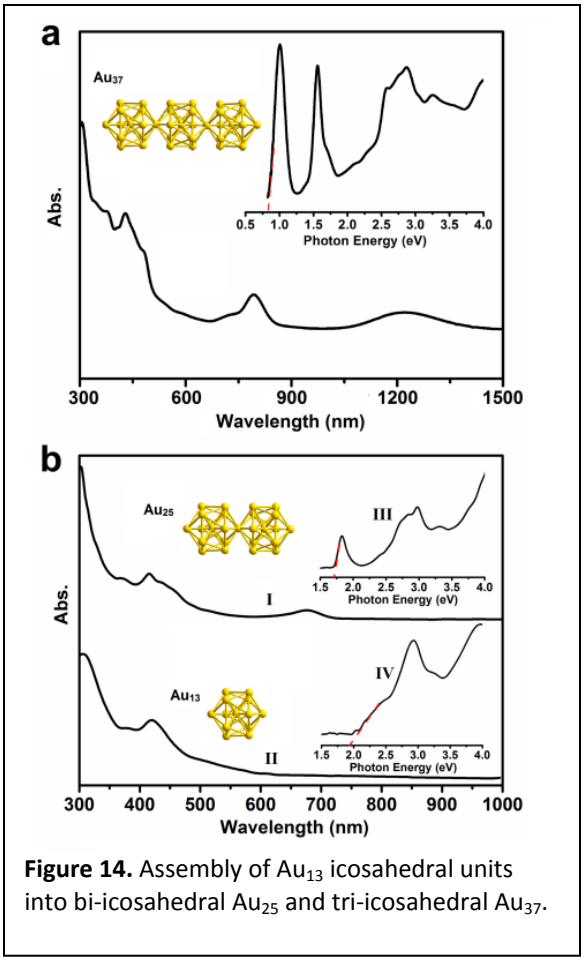

Figure 14. Assembly of Au_{13} icosahedral units into bi-icosahedral Au_{25} and tri-icosahedral Au_{37}.

In another case, we demonstrated a controlled assembly of 13-atom icosahedral building blocks into linear superstructures, such as tri-icosahedral $[Au_{37}(PPh_3)_{10}(SR)_{10}X_2]^+$ nanocluster (where SR=thiolate, X=Cl/Br) (work reported in ***ACS Nano* 2015**). This nanocluster shows a rod-like structure assembled from three icosahedral Au_{13} units in a linear fashion (Figure 14). The successful synthesis of this new nanocluster allows us to gain insight into the size, structure and property evolution of gold nanoclusters that are based upon the assembly of icosahedral units—*i.e. cluster of clusters*. Some interesting trends are identified in the evolution from the mono-icosahedral $[Au_{13}(PPh_3)_8X_2]^{3+}$ to the bi-icosahedral $[Au_{25}(PPh_3)_{10}(SC_2H_4Ph)_5X_2]^{2+}$ and to the tri-icosahedral $[Au_{37}(PPh_3)_{10}(SC_2H_4Ph)_{10}X_2]^+$ nanocluster. In particular, we have recently tackled how the electrons of Au_{13}, Au_{25} and Au_{37} nanoclusters flow after photoexcitation and observed an interesting ~100 ps excited state electron localization process in the rod-shaped Au_{37} nanoclusters made up of three icosahedra (work reported in ***PNAS* 2017**). Upon photoexcitation to S_1 electronic state, electrons in Au_{37} undergo ~100 ps localization from the two vertexes of three icosahedrons to one vertex, forming a long lived S_1^* state. Such phenomenon is not observed in Au_{25} (dimer) and Au_{13} (monomer). We have further investigated the temperature dependence on the localization process, which proves it is thermally-driven. Two excited state vibration modes with frequencies of 20 cm^{-1} and 70 cm^{-1} observed in the kinetic traces are assigned to the axial and radial breathing modes, respectively. The electron-localization is ascribed to the structural distortion of Au_{37} in the excited state induced by the strong coherent vibrations. The observed electron localization phenomenon provides new physical insight into one-dimensional gold nanoclusters and other nanostructures, which will advance their applications in nonlinear optics and energy harvesting.

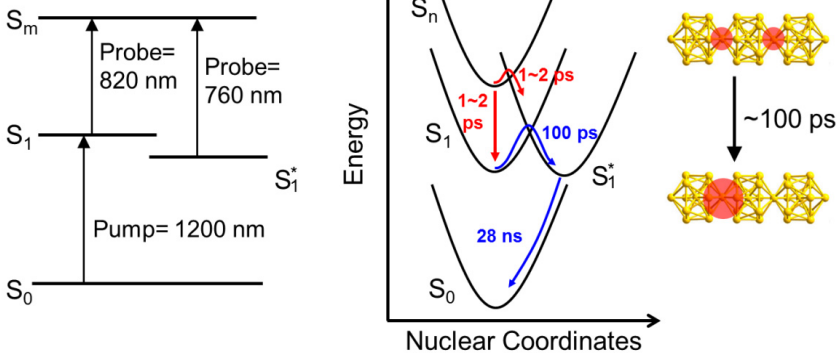

8. Toward the tailoring chemistry of nanoclusters for enhancing functionalities

In recent work, we have developed a site-specific tailoring method for exchanging the surface motif of the 23-atom (Au_{23}) nanocluster and obtained largely enhanced photoluminescence by 10 times (***Science Advances* 2017**). Generally, the structure of nanoclusters consists of an inorganic core and a surface layer, with the latter part protecting the core. The two parts are integrated and cannot simply be taken apart, thus it is very hard to map out which part plays what role. We devised a strategy of performing *site-specific* tailoring of the particle structure and watching how the tailoring of the special part changes the properties of the particle. The present work on thiolate-protected Au_{23} nanocluster is the first example of realizing such a "surgery" on nanoclusters. While in organic chemistry it has been quite mature to perform such tailoring (e.g. changing an –OH group to –COOH on an organic molecule without changing the major carbon bone of the molecule), nanochemistry is still far from that level of structural tailoring at specific sites without changing the other parts of the particle. This work constitutes a major step toward the development of atomically precise, versatile nanochemistry for precise tailoring of the nanocluster structure for controlling the functionalities.

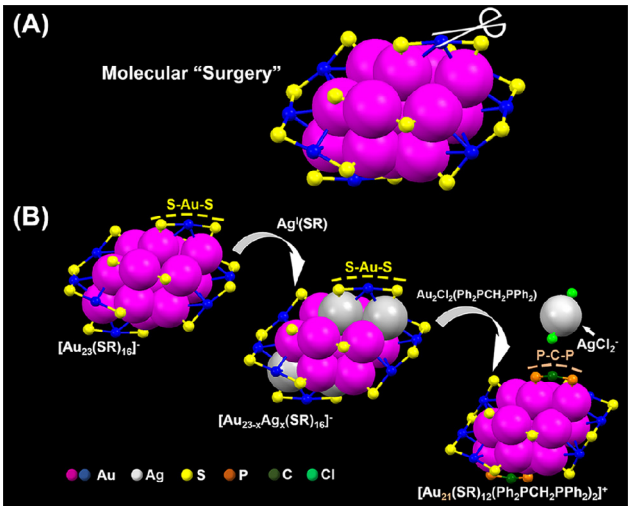

Publications that acknowledged the AF grant:

1. Observation of Body-Centered Cubic Gold Nanocluster. Chao Liu, Tao Li, Gao Li, Katsuyuki Nobusada, Chenjie Zeng, Guangsheng Pang, Nathaniel L. Rosi, and Rongchao Jin. ***Angew. Chem. Int. Ed*.** 2015, 54, 9826–9829.
2. Efficient Electrochemical CO_2 Conversion Powered by Renewable Energy. Douglas R. Kauffman, Jay Thakkar, Rajan Siva, Christopher Matranga, Paul R. Ohodnicki, Chenjie Zeng, and Rongchao Jin. ***ACS Appl. Mater. Interfaces*** 2015, *7*, 15626–15632.
3. Transformation Chemistry of Gold Nanoclusters: From One Stable Size to Another. Chenjie Zeng, Yuxiang Chen, Anindita Das, and Rongchao Jin. ***J. Phys. Chem. Lett.*** 2015, *6*, 2976–2986.
4. Tri-icosahedral Gold Nanocluster $[Au_{37}(PPh_3)_{10}(SC_2H_4Ph)_{10}X_2]^+$: Linear Assembly of Icosahedral Building Blocks. Renxi Jin, § Chong Liu, Shuo Zhao, Anindita Das, Hongzhu Xing, Chakicherla Gayathri, Yan Xing, Nathaniel L. Rosi, Roberto R. Gil, and Rongchao Jin. ***ACS Nano*** 2015, *9*, 8530–8536.
5. Crystal Structure of Barrel-shaped Chiral Au_{130}(*p*-MBT)$_{50}$ Nanocluster. Yuxiang Chen, Chenjie Zeng, Chong Liu, Kristin Kirschbaum, Chakicherla Gayathri, Roberto R. Gil, Nathaniel L. Rosi, and Rongchao Jin, ***J. Am. Chem. Soc.*** 2015, *137*, 10076-10079.
6. Gold Tetrahedra Coil up: Kekulé-like and Double Helical Superstructures. Chenjie Zeng, Yuxiang Chen, Chong Liu, Katsuyuki Nobusada, Nathaniel L. Rosi, and Rongchao Jin, ***Science Advances***, 2015, *1*, e1500425.
7. Isomerism in $Au_{28}(SR)_{20}$ Nanocluster and Stable Structures. Yuxiang Chen, Chong Liu, Qing Tang, Chenjie Zeng, Tatsuya Higaki, Anindita Das, De-en Jiang, Nathaniel L. Rosi, and Rongchao Jin. ***J. Am. Chem. Soc.*** 2016, *138*, 1482–1485.

8. Gold Quantum Boxes: On the Periodicities and the Quantum Confinement in the Au_{28}, Au_{36}, Au_{44} and Au_{52} Magic Series. Zeng, Chenjie; Chen, Yuxiang; Iida, Kenji; Nobusada, Katsuyuki; Kirschbaum, Kristin; Lambright, Kelly; Jin, Rongchao. ***J. Am. Chem. Soc.*** 2016, *138*, 3950–3953.

9. Effects of single atom doping on the ultrafast electron dynamics of $M_1Au_{24}(SR)_{18}$ (M = Pd, Pt) nanoclusters. Meng Zhou, Huifeng Qian, Matthew Y. Sfeir, Katsuyuki Nobusada and Rongchao Jin, ***Nanoscale*** 2016, *8*, 7163-7171.

10. Heavily doped $Au_{25-x}Ag_x(SC_6H_{11})_{18}^-$ nanoclusters: silver goes from the core to the surface. Qi Li, Shuxin Wang, Kristin Kirschbaum, Kelly Lambright, Anindita Das and Rongchao Jin, ***Chem. Commun.***, 2016, 52, 5194-5197.

11. Controlling the Atomic Structure of Au_{30} Nanoclusters by a Ligand-Based Strategy. Tatsuya Higaki, Chong Liu, Chenjie Zeng, Renxi Jin, Yuxiang Chen, Nathaniel L. Rosi, and Rongchao Jin, ***Angew. Chem. Int. Ed.*** 2016, *55*, 6694–6697.

12. Ultrasmall Palladium Nanoclusters as Effective Catalyst for Oxygen Reduction Reaction. Shuo Zhao, Hui Zhang, Stephen D. House, Renxi Jin, Judith Yang, Rongchao Jin. ***ChemElectroChem*** 2016, *3*, 1225-1229.

13. Atomic Structure of Self-Assembled Monolayer of Thiolates on a Tetragonal Au_{92} Nanocrystal. Chenjie Zeng, Chong Liu, Yuxiang Chen, Nathaniel L. Rosi, and Rongchao Jin. ***J. Am. Chem. Soc.*** 2016, 138, 8710–8713.

14. Silicon Nanoparticles with Surface Nitrogen: 90% Quantum Yield with Narrow Luminescence Bandwidth (FWHM~40 nm) and the General Ligand Structure Based PL Energy Law. Qi Li, Meng Zhou, Hadi Abroshan, Jingchun Huang, Hyung J. Kim, Zhengzhong Shao and Rongchao Jin. ***ACS Nano*** 2016, *10*, 8385–8393.

15. Evolution from the Plasmon to Exciton State in Ligand-Protected Atomically Precise Gold Nanoparticles. Zhou, M.; Zeng, C.; Chen, Y.; Zhao, S.; Sfeir, M. Y.; Zhu, M; Jin, R. ***Nat. Commun.*** 2016, *7*, 13240.

16. Titania-Supported Palladium/Strontium Nanoparticles (Pd/Sr-NPs@P25) for Photocatalytic H_2 Production from Water Splitting. Hussain, Ejaz; Majeed, Imran; Nadeem, M. Amtiaz; Badshah, Amin; Chen, Yuxiang; Nadeem, Muhammad Arif; Jin, Rongchao. ***J. Phys. Chem. C*** 2016, *120*, 17205−17213.

17. Controlling the Crystalline Phases (FCC, HCP and BCC) of Thiolate-Protected Gold Nanoclusters by Ligand-Based Strategies. Tatsuya Higaki, Chenjie Zeng, Yuxiang Chen, Ejaz Hussaina, and Rongchao Jin. ***CrystEngComm.*** 2016, *18*, 6979-6986.

18. Characterization of Emissive States for Structurally Precise $Au_{25}(SC_8H_9)_{18}^0$ Monolayer-Protected Gold Nanoclusters Using Magnetophotoluminescence Spectroscopy. Green, Thomas; Herbert, Patrick; Yi, Chongyue; Zeng, Chenjie; McGill, Stephen; Jin, Rongchao; Knappenberger, Kenneth. ***J. Phys. Chem. C*** 2016, 120, 17784-17790.

19. Atomically Precise Colloidal Metal Nanoclusters and Nanoparticles: Fundamentals and Opportunities. Rongchao Jin, Chenjie Zeng, Meng Zhou, Yuxiang Chen. ***Chem. Rev.*** 2016, *116*, 10346–10413.

20. Emergence of hierarchical structural complexities in nanoparticles and their assembly. Chenjie Zeng, Yuxiang Chen, Kristin Kirschbaum, Kelly J. Lambright, Rongchao Jin. ***Science*** 2016, *354*, 1580-1584.

21. Ultrafast Relaxation Dynamics of $Au_{38}(SC_2H_4Ph)_{24}$ Nanoclusters and Effects of Structural Isomerism. Zhou, Meng; Tian, Shubo; Zeng, Chenjie; Sfeir, Matthew; Wu, Zhikun; Jin, Rongchao. ***J. Phys. Chem. C*** 2016, *121*, 10686–10693.

22. The tetrahedral structure and luminescence properties of Bi-metallic Pt1Ag28(SR)18(PPh3)4 nanocluster. Xi Kang, Meng Zhou, Shuxin Wang, Shan Jin, Guodong Sun, Manzhou Zhu* and Rongchao Jin*. ***Chem. Sci.***, 2017, 8, 2581-2587.

23. Gold Nanoclusters Promote Electrocatalytic Water Oxidation at the Nanocluster/$CoSe_2$ Interface. Shuo Zhao, Renxi Jin, Hadi Abroshan, Chenjie Zeng, Hui Zhang, Stephen D. House, Eric Gottlieb, Hyung J. Kim, Judith C. Yang and Rongchao Jin, ***J. Am. Chem. Soc***, 2017, 139, 1077–1080.

24. Surface Engineering of $Au_{36}(SR)_{24}$ Nanoclusters for Photoluminescence Enhancement. Ashley Kim, Chenjie Zeng, Meng Zhou, Rongchao Jin. ***Part. Part. Syst. Charact.*** 2017, 34, 1600388. DOI: 10.1002/ppsc.201600388

25. Molecular "Surgery" on a 23-Gold-Atom Nanoparticle. Qi Li, Tian-Yi Luo, Michael G. Taylor, Shuxin Wang, Xiaofan Zhu, Yongbo Song, Giannis Mpourmpakis, Nathaniel L. Rosi and Rongchao Jin. ***Science Advances*** 2017, *3*, e1603193.

26. Oxidation-Induced Transformation of Eight-Electron Gold Nanoclusters: $[Au_{23}(SR)_{16}]^-$ to $[Au_{28}(SR)_{20}]^0$. Tatsuya Higaki, Chong Liu, Yuxiang Chen, Shuo Zhao, Chenjie Zeng, Renxi Jin, Shuxin Wang, Nathaniel L. Rosi, and Rongchao Jin. ***J. Phys. Chem. Lett.***, 2017, 8, 866–870.

27. Chiral Gold Nanoclusters: Atomic Level Origins of Chirality. Zeng, Chenjie; Jin, Rongchao. ***Chem. Asian J.*** 2017, *12*, 1839-1850.

28. Electron Localization in Rod-Shaped Tri-icosahedral Gold Nanocluster. Meng Zhou, Renxi Jin, Matthew Y. Sfeir, Yuxiang Chen, Yongbo Song, Rongchao Jin. ***Proc. Natl. Acad. Sci. USA***, 2017, *114*, E4697–E4705.

29. Site-selective Substitution of Gold Atoms in the $Au_{24}(SR)_{20}$ Nanocluster by Silver. Qi Li; Michael G Taylor; Kristin Kirschbaum; Kelly Lambright; Xiaofan Zhu; Giannis Mpourmpakis; Rongchao Jin. ***Journal of Colloid and Interface Science*** 2017, 505, 1202-1207.

30. Tailoring the Structure of 58-Electron Gold Nanoclusters: $Au_{103}S_2(S\text{-}Nap)_{41}$ and its Implications. Higaki, Tatsuya; Liu, Chong; Zhou, Meng; Luo, Tian-Yi; Rosi, Nathaniel; Jin, Rongchao. ***J. Am. Chem. Soc***, 2017, *139*, 9994–10001.

31. Atomically Precise Gold Nanoclusters Accelerate Hydrogen Evolution over MoS_2 Nanosheets: The Dual Interfacial Effect. Zhao, Shuo; Jin, Renxi; Song, Yongbo; Zhang, Hui; House, Stephen D.; Yang, Judith C.; Jin, Rongchao. ***Small***, 2017, 13, DOI: 10.1002/smll.201701519.

32. High-throughput, Semi-automated Quantitative STEM Atom-Counting in Supported Metal Nanoparticles Using a Conventional TEM/STEM. Stephen D. Housea, Yuxiang Chen, Rongchao Jin, and Judith C. Yang. ***Ultramicroscopy*** 2017, *182*, 145-155.

33. Bonding properties of FCC-like $Au_{44}(SR)_{28}$ clusters from X-ray absorption spectroscopy. Yang, R Rui; Chevrier, Daniel M.; Zeng, Chenjie; Jin, Rongchao; Zhang, Peng. ***Canadian J. Chem.*** 2017, 95, 1220-1224.

34. Evolution of Excited State Dynamics in Periodic Au_{28}, Au_{36}, Au_{44} and Au_{52} Nanoclusters. Meng Zhou, Chenjie Zeng, Matthew Y. Sfeir, Mircea Cotlet, Kenji Iida, Katsuyuki Nobusada, Rongchao Jin. ***J. Phys. Chem. Lett.*** 2017, *8*, 4023–4030.

35. Photoluminescence from colloidal silicon nanoparticles: significant effect of surface. Qi Li and Rongchao Jin. ***Nanotech. Rev.***, 2017, *6*, 601-612.

36. Electronic Transitions in Highly Symmetric Au_{130} Nanoclusters by Spectroelectrochemistry and Ultrafast Spectroscopy. Padelford, Jonathan; Zhou, Meng; Chen, Yuxiang; Jin, Rongchao; Wang, Gangli. Submitted to ***J. Phys. Chem.*** **C** 2017, *121*, 21217-21224.

37. Controlling Ag-Doping in $[Ag_xAu_{25-x}(SC_6H_{11})_{18}]^-$ Nanoclusters, Cryogenic Optical, Electronic and Electrocatalytic Properties. Renxi Jin, Shuo Zhao, Chong Liu, Meng Zhou, Gihan Panapitiya, Yan Xing, Nathaniel L. Rosi, James P. Lewis and Rongchao Jin. ***Nanoscale*** 2017, *9*, 19183-19190.

38. On the Non-Metallicity of 2.2 nm $Au_{246}(SR)_{80}$ Nanoclusters. Meng Zhou, Chenjie Zeng, Yongbo Song, Jonathan W. Padelford, Gangli Wang, Matthew Y. Sfeir, Tatsuya Higaki, and Rongchao Jin. ***Angew. Chem. Int. Ed.*** 2017, 56, 16257-16261.

39. Ligand- and Solvent-Dependent Electronic Relaxation Dynamics of $Au_{25}(SR)_{18}^-$ Monolayer-Protected Clusters. Yi, Chongyue; Zheng, Hongjun; Herbert, Patrick J.; Chen, Yuxiang; Jin, Rongchao; Knappenberger, Kenneth L., Jr. ***J. Phys. Chem. C***, 2017, 121, 24894-24902.

40. Reconstructing the Surface of Gold Nanoclusters by Cadmium Doping. Qi Li, Kelly J. Lambright, Michael G. Taylor, Kristin Kirschbaum, Tian-Yi Luo, Jianbo Zhao, Giannis Mpourmpakis, Soumitra Mokashi-Punekar, Nathaniel L. Rosi, and Rongchao Jin. ***J. Am. Chem. Soc.***, 2017, 139, 17779–17782.

41. Opportunities and Challenges in CO_2 Reduction by Gold and Silver-based Electrocatalysts: From Bulk Metals to Nanoparticles and Atomically Precise Nanoclusters. Shuo Zhao, Renxi Jin, and Rongchao Jin. ***ACS Energy Lett.*** 2018, 3, 452-462.

42. Chiral Ag_{23} nanocluster with open shell electronic structure and helical face-centered cubic framework. Chao Liu, Tao Li, Hadi Abroshan, Zhimin Li, Chen Zhang, Hyung J. Kim, Gao Li & Rongchao Jin. ***Nature Communications*** 2018, 9, 744.

43. Excited-State Behaviors of $M_1Au_{24}(SR)_{18}$ Nanoclusters: The Number of Valence Electrons Matters. Meng Zhou, Chuanhao Yao, Matthew Y. Sfeir, Tatsuya Higaki, Zhikun Wu, and Rongchao Jin. ***J. Phys. Chem. C*** 2018, Article ASAP, DOI: 10.1021/acs.jpcc.7b11057.

44. Structural Evolution Patterns of FCC-Type Gold Nanoclusters. Tatsuya Higaki, Rongchao Jin. ***Acta Physico-Chimica Sinca***, 2018, 34, 755-761. doi: 10.3866/PKU.WHXB201801191.

45. Influence of Atomic-Level Morphology on Catalysis: The Case of Sphere and Rod-Like Gold Nanoclusters for CO_2 Electroreduction. Shuo Zhao, Natalie Austin, Mo Li, Yongbo Song, Stephen D. House, Stefan Bernhard, Judith C. Yang, Giannis Mpourmpakis, and Rongchao Jin. ***ACS Catal.***, 2018, 8, 4996–5001.

46. Sharp Transition from Nonmetallic Au_{246} to Metallic Au_{279} with Nascent Surface Plasmon Resonance. Higaki, Tatsuya; Zhou, Meng; Lambright, Kelly; Kirschbaum, Kristin; Sfeir, Matthew Y.; Jin, Rongchao. ***J. Am. Chem. Soc.***, 2018, 140, 5691–5695.

AFOSR Deliverables Submission Survey

Response ID:10077 Data

1.

Report Type

Final Report

Primary Contact Email

Contact email if there is a problem with the report.

rongchao@andrew.cmu.edu

Primary Contact Phone Number

Contact phone number if there is a problem with the report

1(412)2689448

Organization / Institution name

Carnegie Mellon University

Grant/Contract Title

The full title of the funded effort.

Atomically Precise Metal Nanoclusters: Structure, Dynamics and Catalysis

Grant/Contract Number

AFOSR assigned control number. It must begin with "FA9550" or "F49620" or "FA2386".

FA9550-15-1-0154

Principal Investigator Name

The full name of the principal investigator on the grant or contract.

Rongchao Jin

Program Officer

The AFOSR Program Officer currently assigned to the award

Dr. Michael Berman

Reporting Period Start Date

04/15/2015

Reporting Period End Date

04/14/2018

Abstract

We have fulfilled the central goal of our project, which is to investigate the structure and properties of atomically precise, ligand-protected metal nanoclusters in the size range from tens to hundreds of atoms. Such new materials have found major applications in catalysis for energy conversion, including CO2 reduction to fuels and water splitting to H2. The evolution of electronic and optical properties with cluster size is discovered to impact the catalytic reactivity. The correlations between the structure and catalytic reactivity have been mapped out. We have developed capabilities for controlling gold and bimetallic nanoclusters at the single-atom level (including heteroatom doping). Such capabilities are particularly important for designing atom-efficient new materials with tailored properties to meet specific energy and catalysis needs. Characterization of the atomic structures of nanoclusters enabled fundamental understanding of the mechanisms of the catalyzed reactions. Heteroatom substitution in gold nanoclusters allowed us to probe the atomic-level sensitivity of the nanocluster's electronic, optical and catalytic properties, and also to impart the nanocluster with new properties. We have gained insights into how the structure of nanocluster catalysts can be manipulated for catalytic processes. Such new insights will benefit rational design of highly efficient catalysts.

Distribution Statement

This is block 12 on the SF298 form.

Distribution A - Approved for Public Release

Explanation for Distribution Statement

If this is not approved for public release, please provide a short explanation. E.g., contains proprietary information.

SF298 Form

Please attach your SF298 form. A blank SF298 can be found here. Please do not password protect or secure the PDF The maximum file size for an SF298 is 50MB.

sf298.pdf

Upload the Report Document. File must be a PDF. Please do not password protect or secure the PDF . The maximum file size for the Report Document is 50MB.

FA9550-15-1-0154_final_report.pdf

Upload a Report Document, if any. The maximum file size for the Report Document is 50MB.

Archival Publications (published) during reporting period:

Publications that acknowledged the AF grant:

1. Observation of Body-Centered Cubic Gold Nanocluster. Chao Liu, Tao Li, Gao Li, Katsuyuki Nobusada, Chenjie Zeng, Guangsheng Pang, Nathaniel L. Rosi, and Rongchao Jin. Angew. Chem. Int. Ed. 2015, 54, 9826–9829.

2. Efficient Electrochemical CO2 Conversion Powered by Renewable Energy. Douglas R. Kauffman, Jay Thakkar, Rajan Siva, Christopher Matranga, Paul R. Ohodnicki, Chenjie Zeng, and Rongchao Jin. ACS Appl. Mater. Interfaces 2015, 7, 15626–15632.

3. Transformation Chemistry of Gold Nanoclusters: From One Stable Size to Another. Chenjie Zeng, Yuxiang Chen, Anindita Das, and Rongchao Jin. J. Phys. Chem. Lett. 2015, 6, 2976–2986.

4. Tri-icosahedral Gold Nanocluster [Au37(PPh3)10(SC2H4Ph)10X2]+: Linear Assembly of Icosahedral Building Blocks. Renxi Jin, § Chong Liu, Shuo Zhao, Anindita Das, Hongzhu Xing, Chakicherla Gayathri, Yan Xing, Nathaniel L. Rosi, Roberto R. Gil, and Rongchao Jin. ACS Nano 2015, 9, 8530–8536.

5. Crystal Structure of Barrel-shaped Chiral Au130(p-MBT)50 Nanocluster. Yuxiang Chen, Chenjie Zeng, Chong Liu, Kristin Kirschbaum, Chakicherla Gayathri, Roberto R. Gil, Nathaniel L. Rosi, and Rongchao Jin, J. Am. Chem. Soc. 2015, 137, 10076-10079.

6. Gold Tetrahedra Coil up: Kekulé-like and Double Helical Superstructures. Chenjie Zeng, Yuxiang Chen, Chong Liu, Katsuyuki Nobusada, Nathaniel L. Rosi, and Rongchao Jin, Science Advances, 2015, 1, e1500425.

7. Isomerism in Au28(SR)20 Nanocluster and Stable Structures. Yuxiang Chen, Chong Liu, Qing Tang, Chenjie Zeng, Tatsuya Higaki, Anindita Das, De-en Jiang, Nathaniel L. Rosi, and Rongchao Jin. J. Am. Chem. Soc. 2016, 138, 1482–1485.

8. Gold Quantum Boxes: On the Periodicities and the Quantum Confinement in the Au28, Au36, Au44 and Au52 Magic Series. Zeng, Chenjie; Chen, Yuxiang; Iida, Kenji; Nobusada, Katsuyuki; Kirschbaum, Kristin; Lambright, Kelly; Jin, Rongchao. J. Am. Chem. Soc. 2016, 138, 3950–3953.

9. Effects of single atom doping on the ultrafast electron dynamics of M1Au24(SR)18 (M = Pd, Pt) nanoclusters. Meng Zhou, Huifeng Qian, Matthew Y. Sfeir, Katsuyuki Nobusada and Rongchao Jin, Nanoscale 2016, 8, 7163-7171.

10. Heavily doped Au25–xAgx(SC6H11)18– nanoclusters: silver goes from the core to the surface. Qi Li, Shuxin Wang, Kristin Kirschbaum, Kelly Lambright, Anindita Das and Rongchao Jin, Chem. Commun., 2016, 52, 5194-5197.

11. Controlling the Atomic Structure of Au30 Nanoclusters by a Ligand-Based Strategy. Tatsuya Higaki, Chong Liu, Chenjie Zeng, Renxi Jin, Yuxiang Chen, Nathaniel L. Rosi, and Rongchao Jin, Angew. Chem. Int. Ed. 2016, 55, 6694–6697.

12. Ultrasmall Palladium Nanoclusters as Effective Catalyst for Oxygen Reduction Reaction. Shuo Zhao, Hui Zhang, Stephen D. House, Renxi Jin, Judith Yang, Rongchao Jin. ChemElectroChem 2016, 3, 1225-1229.

13. Atomic Structure of Self-Assembled Monolayer of Thiolates on a Tetragonal Au92 Nanocrystal. Chenjie Zeng, Chong Liu, Yuxiang Chen, Nathaniel L. Rosi, and Rongchao Jin. J. Am. Chem. Soc. 2016, 138, 8710–8713.
14. Silicon Nanoparticles with Surface Nitrogen: 90% Quantum Yield with Narrow Luminescence Bandwidth (FWHM~40 nm) and the General Ligand Structure Based PL Energy Law. Qi Li, Meng Zhou, Hadi Abroshan, Jingchun Huang, Hyung J. Kim, Zhengzhong Shao and Rongchao Jin. ACS Nano 2016, 10, 8385–8393.
15. Evolution from the Plasmon to Exciton State in Ligand-Protected Atomically Precise Gold Nanoparticles. Zhou, M.; Zeng, C.; Chen, Y.; Zhao, S.; Sfeir, M. Y.; Zhu, M; Jin, R. Nat. Commun. 2016, 7, 13240.
16. Titania-Supported Palladium/Strontium Nanoparticles (Pd/Sr-NPs@P25) for Photocatalytic H2 Production from Water Splitting. Hussain, Ejaz; Majeed, Imran; Nadeem, M. Amtiaz; Badshah, Amin; Chen, Yuxiang; Nadeem, Muhammad Arif; Jin, Rongchao. J. Phys. Chem. C 2016, 120, 17205–17213.
17. Controlling the Crystalline Phases (FCC, HCP and BCC) of Thiolate-Protected Gold Nanoclusters by Ligand-Based Strategies. Tatsuya Higaki, Chenjie Zeng, Yuxiang Chen, Ejaz Hussaina, and Rongchao Jin. CrystEngComm. 2016, 18, 6979-6986.
18. Characterization of Emissive States for Structurally Precise Au25(SC8H9)180 Monolayer-Protected Gold Nanoclusters Using Magnetophotoluminescence Spectroscopy. Green, Thomas; Herbert, Patrick; Yi, Chongyue; Zeng, Chenjie; McGill, Stephen; Jin, Rongchao; Knappenberger, Kenneth. J. Phys. Chem. C 2016, 120, 17784-17790.
19. Atomically Precise Colloidal Metal Nanoclusters and Nanoparticles: Fundamentals and Opportunities. Rongchao Jin, Chenjie Zeng, Meng Zhou, Yuxiang Chen. Chem. Rev. 2016, 116, 10346–10413.
20. Emergence of hierarchical structural complexities in nanoparticles and their assembly. Chenjie Zeng, Yuxiang Chen, Kristin Kirschbaum, Kelly J. Lambright, Rongchao Jin. Science 2016, 354, 1580-1584.
21. Ultrafast Relaxation Dynamics of Au38(SC2H4Ph)24 Nanoclusters and Effects of Structural Isomerism. Zhou, Meng; Tian, Shubo; Zeng, Chenjie; Sfeir, Matthew; Wu, Zhikun; Jin, Rongchao. J. Phys. Chem. C 2016, 121, 10686–10693.
22. The tetrahedral structure and luminescence properties of Bi-metallic Pt1Ag28(SR)18(PPh3)4 nanocluster. Xi Kang, Meng Zhou, Shuxin Wang, Shan Jin, Guodong Sun, Manzhou Zhu* and Rongchao Jin*. Chem. Sci., 2017, 8, 2581-2587.
23. Gold Nanoclusters Promote Electrocatalytic Water Oxidation at the Nanocluster/CoSe2 Interface. Shuo Zhao, Renxi Jin, Hadi Abroshan, Chenjie Zeng, Hui Zhang, Stephen D. House, Eric Gottlieb, Hyung J. Kim, Judith C. Yang and Rongchao Jin, J. Am. Chem. Soc, 2017, 139, 1077–1080.
24. Surface Engineering of Au36(SR)24 Nanoclusters for Photoluminescence Enhancement. Ashley Kim, Chenjie Zeng, Meng Zhou, Rongchao Jin. Part. Part. Syst. Charact. 2017, 34, 1600388. DOI: 10.1002/ppsc.201600388
25. Molecular "Surgery" on a 23-Gold-Atom Nanoparticle. Qi Li, Tian-Yi Luo, Michael G. Taylor, Shuxin Wang, Xiaofan Zhu, Yongbo Song, Giannis Mpourmpakis, Nathaniel L. Rosi and Rongchao Jin. Science Advances 2017, 3, e1603193.
26. Oxidation-Induced Transformation of Eight-Electron Gold Nanoclusters: [Au23(SR)16]– to [Au28(SR)20]0. Tatsuya Higaki, Chong Liu, Yuxiang Chen, Shuo Zhao, Chenjie Zeng, Renxi Jin, Shuxin Wang, Nathaniel L. Rosi, and Rongchao Jin. J. Phys. Chem. Lett., 2017, 8, 866–870.
27. Chiral Gold Nanoclusters: Atomic Level Origins of Chirality. Zeng, Chenjie; Jin, Rongchao. Chem. Asian J. 2017, 12, 1839-1850.
28. Electron Localization in Rod-Shaped Tri-icosahedral Gold Nanocluster. Meng Zhou, Renxi Jin, Matthew Y. Sfeir, Yuxiang Chen, Yongbo Song, Rongchao Jin. Proc. Natl. Acad. Sci. USA, 2017, 114, E4697–E4705.
29. Site-selective Substitution of Gold Atoms in the Au24(SR)20 Nanocluster by Silver. Qi Li; Michael G Taylor; Kristin Kirschbaum; Kelly Lambright; Xiaofan Zhu; Giannis Mpourmpakis; Rongchao Jin. Journal of Colloid and Interface Science 2017, 505, 1202-1207.
30. Tailoring the Structure of 58-Electron Gold Nanoclusters: Au103S2(S-Nap)41 and its Implications. Higaki, Tatsuya; Liu, Chong; Zhou, Meng; Luo, Tian-Yi; Rosi, Nathaniel; Jin, Rongchao. J. Am. Chem. Soc, 2017, 139, 9994–10001.

31. Atomically Precise Gold Nanoclusters Accelerate Hydrogen Evolution over MoS2 Nanosheets: The Dual Interfacial Effect. Zhao, Shuo; Jin, Renxi; Song, Yongbo; Zhang, Hui; House, Stephen D.; Yang, Judith C.; Jin, Rongchao. Small, 2017, 13, DOI: 10.1002/smll.201701519.
32. High-throughput, Semi-automated Quantitative STEM Atom-Counting in Supported Metal Nanoparticles Using a Conventional TEM/STEM. Stephen D. Housea, Yuxiang Chen, Rongchao Jin, and Judith C. Yang. Ultramicroscopy 2017, 182, 145-155.
33. Bonding properties of FCC-like Au44(SR)28 clusters from X-ray absorption spectroscopy. Yang, R Rui; Chevrier, Daniel M.; Zeng, Chenjie; Jin, Rongchao; Zhang, Peng. Canadian J. Chem. 2017, 95, 1220-1224.
34. Evolution of Excited State Dynamics in Periodic Au28, Au36, Au44 and Au52 Nanoclusters. Meng Zhou, Chenjie Zeng, Matthew Y. Sfeir, Mircea Cotlet, Kenji Iida, Katsuyuki Nobusada, Rongchao Jin. J. Phys. Chem. Lett. 2017, 8, 4023–4030.
35. Photoluminescence from colloidal silicon nanoparticles: significant effect of surface. Qi Li and Rongchao Jin. Nanotech. Rev., 2017, 6, 601-612.
36. Electronic Transitions in Highly Symmetric Au130 Nanoclusters by Spectroelectrochemistry and Ultrafast Spectroscopy. Padelford, Jonathan; Zhou, Meng; Chen, Yuxiang; Jin, Rongchao; Wang, Gangli. Submitted to J. Phys. Chem. C 2017, 121, 21217-21224.
37. Controlling Ag-Doping in [AgxAu25-x(SC6H11)18]– Nanoclusters, Cryogenic Optical, Electronic and Electrocatalytic Properties. Renxi Jin, Shuo Zhao, Chong Liu, Meng Zhou, Gihan Panapitiya, Yan Xing, Nathaniel L. Rosi, James P. Lewis and Rongchao Jin. Nanoscale 2017, 9, 19183-19190.
38. On the Non-Metallicity of 2.2 nm Au246(SR)80 Nanoclusters. Meng Zhou, Chenjie Zeng, Yongbo Song, Jonathan W. Padelford, Gangli Wang, Matthew Y. Sfeir, Tatsuya Higaki, and Rongchao Jin. Angew. Chem. Int. Ed. 2017, 56, 16257-16261.
39. Ligand- and Solvent-Dependent Electronic Relaxation Dynamics of Au25(SR)18- Monolayer-Protected Clusters. Yi, Chongyue; Zheng, Hongjun; Herbert, Patrick J.; Chen, Yuxiang; Jin, Rongchao; Knappenberger, Kenneth L., Jr. J. Phys. Chem. C, 2017, 121, 24894-24902.
40. Reconstructing the Surface of Gold Nanoclusters by Cadmium Doping. Qi Li, Kelly J. Lambright, Michael G. Taylor, Kristin Kirschbaum, Tian-Yi Luo, Jianbo Zhao, Giannis Mpourmpakis, Soumitra Mokashi-Punekar, Nathaniel L. Rosi, and Rongchao Jin. J. Am. Chem. Soc., 2017, 139, 17779–17782.
41. Opportunities and Challenges in CO2 Reduction by Gold and Silver-based Electrocatalysts: From Bulk Metals to Nanoparticles and Atomically Precise Nanoclusters. Shuo Zhao, Renxi Jin, and Rongchao Jin. ACS Energy Lett. 2018, 3, 452-462.
42. Chiral Ag23 nanocluster with open shell electronic structure and helical face-centered cubic framework. Chao Liu, Tao Li, Hadi Abroshan, Zhimin Li, Chen Zhang, Hyung J. Kim, Gao Li & Rongchao Jin. Nature Communications 2018, 9, 744.
43. Excited-State Behaviors of M1Au24(SR)18 Nanoclusters: The Number of Valence Electrons Matters. Meng Zhou, Chuanhao Yao, Matthew Y. Sfeir, Tatsuya Higaki, Zhikun Wu, and Rongchao Jin. J. Phys. Chem. C 2018, Article ASAP, DOI: 10.1021/acs.jpcc.7b11057.
44. Structural Evolution Patterns of FCC-Type Gold Nanoclusters. Tatsuya Higaki, Rongchao Jin. Acta Physico-Chimica Sinca, 2018, 34, 755-761.
45. Influence of Atomic-Level Morphology on Catalysis: The Case of Sphere and Rod-Like Gold Nanoclusters for CO2 Electroreduction. Shuo Zhao, Natalie Austin, Mo Li, Yongbo Song, Stephen D. House, Stefan Bernhard, Judith C. Yang, Giannis Mpourmpakis, and Rongchao Jin. ACS Catal., 2018, 8, 4996–5001.
46. Sharp Transition from Nonmetallic Au246 to Metallic Au279 with Nascent Surface Plasmon Resonance. Higaki, Tatsuya; Zhou, Meng; Lambright, Kelly; Kirschbaum, Kristin; Sfeir, Matthew Y.; Jin, Rongchao. J. Am. Chem. Soc., 2018, 140, 5691–5695.

New discoveries, inventions, or patent disclosures:

Do you have any discoveries, inventions, or patent disclosures to report for this period?

No

Please describe and include any notable dates

Do you plan to pursue a claim for personal or organizational intellectual property?

Changes in research objectives (if any):

Change in AFOSR Program Officer, if any:

Extensions granted or milestones slipped, if any:

AFOSR LRIR Number

LRIR Title

Reporting Period

Laboratory Task Manager

Program Officer

Research Objectives

Technical Summary

Funding Summary by Cost Category (by FY, $K)

	Starting FY	FY+1	FY+2
Salary			
Equipment/Facilities			
Supplies			
Total			

Report Document

Report Document - Text Analysis

Report Document - Text Analysis

Appendix Documents

2. Thank You

E-mail user

Jul 17, 2018 14:29:32 Success: Email Sent to: rongchao@andrew.cmu.edu